Localized or itinerant TiO_3 electrons in $RTiO_3$ perovskites

2005 J. Phys.: Condens. Matter 17 7395

(http://iopscience.iop.org/0953-8984/17/46/023)

INSTITUTE OF PHYSICS PUBLISHING JOURNAL OF PHYSICS: CONDENSED MATTER

J. Phys.: Condens. Matter **17** (2005) 7395–7406 doi:10.1088/0953-8984/17/46/023

Localized or itinerant TiO_3 electrons in $RTiO_3$ perovskites

H D Zhou[1] **and J B Goodenough**

Texas Materials Institute, ETC 9.102, 1 University Station, C2201, University of Texas at Austin, Austin, TX 78712-1063, USA

E-mail: hdzhou@physics.utexas.edu

Received 31 August 2005, in final form 4 October 2005
Published 1 November 2005
Online at stacks.iop.org/JPhysCM/17/7395

Abstract

A reinvestigation of nearly stoichiometric $RTiO_3$ samples shows that (1) the transition from ferromagnetic to antiferromagnetic Ti–O–Ti interactions with increasing R^{3+}-ion radius r_{3+} occurs at $r_{3+} \approx 1.11$ Å where orthorhombic ($Pbnm$) RMO_3 perovskites universally change structure from a cooperative rotation of undistorted to distorted $MO_{6/2}$ octahedra about the orthorhombic b-axis, (2) the size of polaronic holes decreases progressively with r_{3+} from about ten Ti sites in $LaTiO_3$ to small polarons in $GdTiO_3$, (3) the strength of the R–O–Ti interactions increases with the spin of the R^{3+} ion in the ferromagnetic compounds, (4) the saturation magnetization of the ferromagnetic TiO_3 array at 5 K and the Curie temperature T_C both increase with decreasing r_{3+} where the R^{3+} ions have no spin, and (5) there is no evidence of 'cluster-glass' behaviour where there is no variance of the R^{3+}-ion radii. The cooperative Jahn–Teller orbital ordering and small-polaron behaviour of the ferrimagnetic and ferromagnetic compounds would favour localized Ti-3d electrons. However, the lack of saturation to 1 μ_B/Ti of the ferromagnetic TiO_3 array in the absence of a spin on the R^{3+} ion suggests a separation of an orbitally ordered ferromagnetic phase and an orbitally disordered paramagnetic phase.

1. Introduction

All members of the $RTiO_3$ perovskite family (R = rare-earth or Y) have the Ti(IV)/Ti(III) and Ti(III)/Ti(II) redox couples separated by an energy gap that increases from 0.2 eV in antiferromagnetic $LaTiO_3$ to near 1.2 eV in ferromagnetic $YTiO_3$ [1–3]. The heavier rare-earth ions Gd–Yb all exhibit a ferromagnetic TiO_3 array that couples antiparallel to a ferromagnetic component on the rare-earth array to give a net ferrimagnetism below a Curie temperature T_C; the antiferromagnetic R–O–Ti interactions are reported to be weaker than the ferromagnetic Ti–O–Ti interactions [4, 5]. The lighter rare-earth ions Ce–Sm all have an antiferromagnetic

[1] Author to whom any correspondence should be addressed.

TiO_3 array like $LaTiO_3$ below a T_{N1} [6, 7]; the rare-earth moments order independently and antiferromagnetically below a $T_{N2} < T_{N1}$. The Curie temperature T_C decreases with decreasing atomic weight of the R^{3+} ion from Dy to Gd, and T_{N1} increases from Sm to La [2, 8]. The long-range magnetic-ordering temperatures T_{N1} and T_C decrease to below 10 K at the crossover composition $Sm_{0.5}Gd_{0.5}TiO_3$ where there is no long-range orbital ordering [9].

The ferromagnetism of $YTiO_3$ below $T_C \approx 30$ K is the result of G-type orbital ordering below a $T_{OO} > T_C$ of the π-bonding t electron into a yz or zx orbital on alternate Ti(III) ions of the TiO_3 array [10]; the orbital ordering couples half-filled and empty π-bonding t orbitals on neighbouring Ti(III) ions to give ferromagnetic superexchange interactions in accordance with the Goodenough–Kanamori rules. However, at antiphase boundaries, yz–yz or zx–zx interactions between half-filled orbitals introduce an antiferromagnetic coupling across the boundary between ferromagnetic regions, which results in a low remanence [11].

The antiferromagnetic order of $LaTiO_3$ below a $T_{N1} = 140$ K is due to a $TiO_{6/2}$ site deformation from cubic to rhombohedral symmetry that stabilizes an a_1 orbital oriented along its [111] axis [12, 13]; moreover, the magnitude of the site deformation increases abruptly on cooling through T_{N1}. This orbital ordering has no preferred Ti–O–Ti axis and is, therefore, responsible for the G-type antiferromagnetic order found for the lighter R^{3+} ions. Cwik *et al* [12] also observed that both the magnitude of the site deformation and T_{N1} decrease with the size of the R^{3+} ion in the $RTiO_3$ family; the site deformation, but not its cooperative rotation about the orthorhombic ($Pbnm$) b-axis, essentially disappears in the ferromagnetic compositions having a G-type ordering of the occupied yz and zx orbitals. However, left unresolved is whether orbital order drives the site deformation or the site deformation stabilizes the orbital order.

Here we report a reinvestigation of nearly stoichiometric samples of the $RTiO_3$ family to determine (1) the origin of the site deformations, (2) the evolution with R^{3+}-ion radius r_{3+} of the activation energy of polaronic p-type transport in the TiO_3 array, (3) how the strength of the R^{3+}–O–Ti^{3+} spin–spin interaction changes with the spin of the R^{3+} ion in the ferromagnetic compositions, (4) how the saturation magnetization of the TiO_3 array approaches the spin-only value of 1 μ_B/Ti in the absence of a moment on the rare-earth ion, and (5) whether the report by Yoshii *et al* [14] of 'cluster-glass' behaviour in the $R_{1-x}Nd_xTiO_3$ perovskites with R = Ce or Pr is found where there is no variance of the R^{3+}-ion radius.

2. Experimental details

Polycrystalline samples of $RTiO_3$ (R = rare earth or Y) were prepared by solid-state reaction. Stoichiometric mixtures of R_2O_3 or Pr_6O_{11} or Tb_4O_7 and Ti_2O_3 were ground together for each composition; the powders were cold-pressed into pellets, placed into a molybdenum crucible and put into a tube that was then evacuated to $\sim 10^{-6}$ Torr before firing at 1620 °C for 12 h.

A Perkin-Elmer TGA-7 thermogravimetric analyser was used to determine the oxygen content of the samples from the weight gain due to an oxidation of the Ti(III) ions to Ti(IV) on heating to 1000 °C in air. For all samples, the excess oxygen was smaller than 0.4%; they were oxygen-stoichiometric within experimental error.

Powder x-ray diffraction (XRD) patterns were recorded with a Philips PW 1729 powder x-ray diffractometer equipped with a pyrolytic graphite monochromator and Cu Kα radiation (1.540 59 Å); Si was the internal standard. Data were collected in steps of 0.020° over the range $20° \leqslant \theta \leqslant 60°$ with a count time of 20 s per step. Peak profiles for the XRD data were fitted with the program JADE. All samples were single-phase to XRD.

Magnetic susceptibility measurements were made with a Quantum Design dc SQUID magnetometer after cooling in zero field (ZFC) or after cooling in a measuring field (FC) of

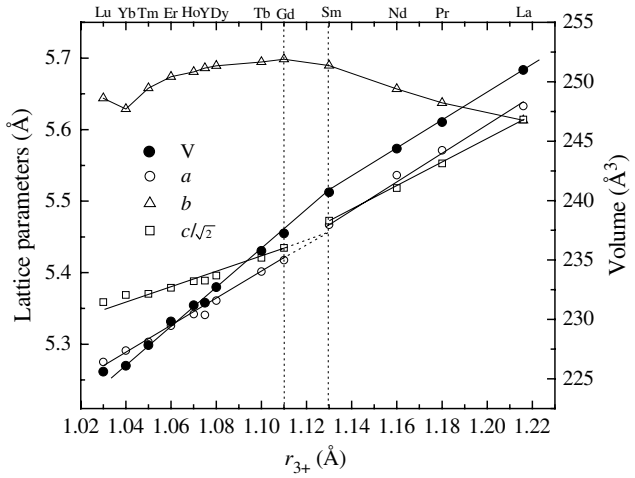

Figure 1. Variation with r_{3+} of the room-temperature lattice parameters of the orthorhombic *Pbnm* $RTiO_3$ perovskites. The dashed lines are guides for the eye.

100 Oe, 1 kOe, or 10 kOe. M–H hysteresis loops of magnetization M versus applied magnetic field H were measured over the range $-5\ \mathrm{T} \leqslant H \leqslant 5\ \mathrm{T}$ at 5 K.

The low-temperature thermoelectric power $\alpha(T)$ was obtained from 80 to 320 K with a laboratory-built apparatus as described elsewhere [15]. The resistivity was measured by a four-probe technique on samples that were cold-pressed as mixed powders. The cold-pressing technique has been described elsewhere [16].

3. Results

All samples of the orthorhombic *Pbnm* perovskite family $RTiO_3$ were single-phase to XRD. Figure 1 displays the room-temperature variation of unit-cell volumes and lattice parameters with the R^{3+}-ion radius r_{3+} as calculated for ninefold oxygen coordination. The lattice parameters also are listed in table 1. The lattice parameter b increases with increasing r_{3+} to $GdTiO_3$, where $r_{3+} = 1.11$ Å; it decreases with a further increase in r_{3+} where $c/a < \sqrt{2}$ is found.

All the $RTiO_3$ samples were p-type semiconductors with a $\rho(T) \sim \exp(E_a/kT)$, where $E_a = \Delta H_m + (\Delta H_t/2)$ is the sum of the motional enthalpy and an enthalpy ΔH_t of trapping at the cation vacancy that created the mobile holes. Figure 2 shows that an $E_a \geqslant 0.23$ eV increases little with decreasing r_{3+} on passing from $GdTiO_3$ to $LuTiO_3$ whereas E_a increases sharply with decreasing r_{3+} on passing from $LaTiO_3$ with $E_a = 0.035$ eV to $GdTiO_3$. From thermoelectric-power measurements $\alpha(T)$, we have shown that the mobile holes in $LaTiO_3$ occupy itinerant-electron clusters containing multiple Ti atoms [11], and the data of figure 2 are consistent with a cluster size that decreases progressively to that of a small polaron as r_{3+} decreases. However, the high resistance of the samples with smaller r_{3+} did not permit a good measure of $\alpha(T)$, so we were unable to determine reliably the separate contributions of ΔH_m and ΔH_t for samples other than $LaTiO_3$ and therefore their separate evolutions with r_{3+}.

The magnetic susceptibilities $1/\chi_m(T)$ and $\chi_m(T)$ for R = La, Pr, Nd, and Sm are shown in figures 3 and 4; data were taken on heating after cooling in zero field (ZFC) and in the measuring field (FC) of $H = 100$ Oe, 1 kOe, or 10 kOe. All samples show a T_{N1} that

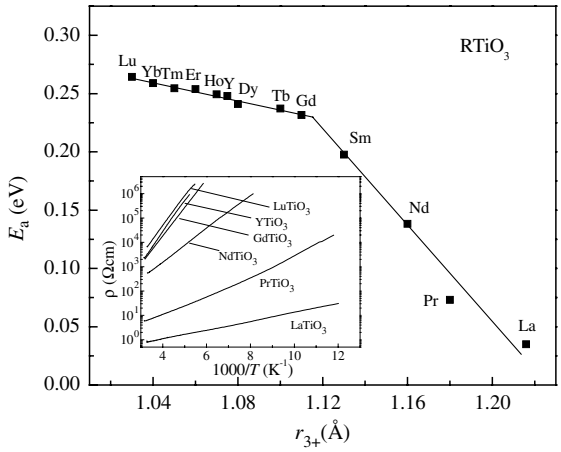

Figure 2. Variation with r_{3+} of the activation energy E_a of the resistivity $\rho(T) \sim \exp(E_a/kT)$ for the p-type $RTiO_3$ perovskites. Inset: $\rho \sim 1/T$ curves for several $RTiO_3$ samples. The straight lines are guides for the eye.

Table 1. Variation with R in $RTiO_3$ of room-temperature lattice parameters.

$RTiO_3$	a (Å)	b (Å)	c (Å)	V (Å^3)
La	5.633(1)	5.613(2)	7.942(2)	251.1
Pr	5.555(2)	5.615(1)	7.821(2)	244.0
Nd	5.524(1)	5.657(1)	7.795(1)	243.6
Sm	5.467(1)	5.669(1)	7.742(1)	240.0
Gd	5.402(2)	5.697(2)	7.680(2)	236.4
Tb	5.384(1)	5.678(1)	7.660(1)	234.2
Dy	5.363(3)	5.689(2)	7.647(1)	233.3
Y	5.341(1)	5.686(2)	7.621(1)	231.4
Ho	5.340(2)	5.689(2)	7.622(1)	231.5
Er	5.320(3)	5.674(3)	7.609(2)	229.7
Tm	5.303(1)	5.658(1)	7.597(3)	228.0
Yb	5.291(1)	5.629(1)	7.595(1)	226.0
Lu	5.275(1)	5.644(1)	7.581(2)	225.7

decreases progressively from 140 K in $LaTiO_3$ to about 120 K in $PrTiO_3$, 110 K in $NdTiO_3$, and 70 K in $SmTiO_3$ as determined by a divergence of the FC and ZFC curves below T_{N1} in $H = 100$ Oe. This divergence is caused by a weak ferromagnetic component due to an antisymmetric exchange contribution $D_{ij} \cdot S_i \times S_j$ with D_{ij} parallel to the b axis, which is associated with a canting of the antiferromagnetically coupled spins of the TiO_3 array.

Where the R^{3+} ions have a large moment, these moments dominate the $1/\chi_m(T)$ curves. Nevertheless, a deviation from Curie–Weiss behaviour below a T_1 is found for all the heavier R^{3+} ions, figure 5; for these compounds, T_1 decreases systematically with decreasing r_{3+} whereas T_C varies irregularly with r_{3+}, figure 6. Magnetic parameters are listed in table 2.

Figure 8 shows the M–H hysteresis loops taken at 5 K for the heavier R^{3+} ions.

4. Discussion

In figure 1, the linear increase of a and c and the decrease in $c/a > \sqrt{2}$ with increasing $r_{3+} < 1.11$ Å are consistent with a cooperative rotation of the $TiO_{6/2}$ octahedra about

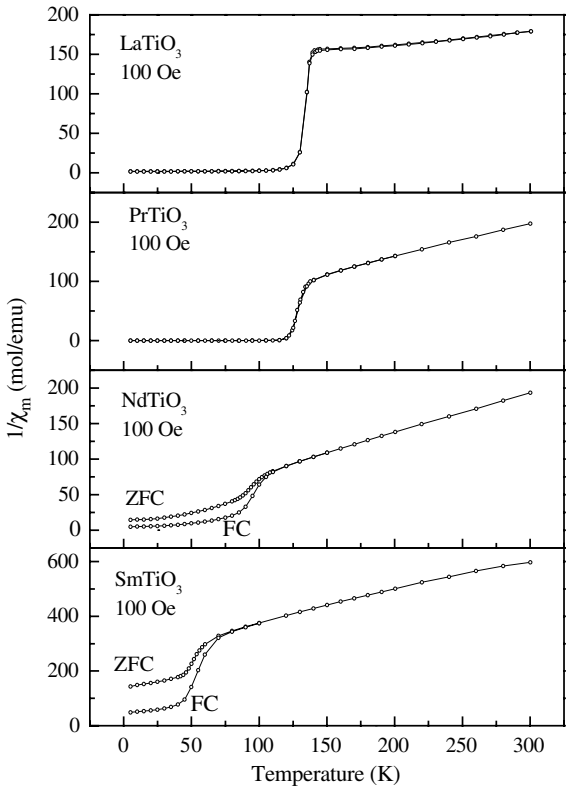

Figure 3. Inverse molar magnetic susceptibility $1/\chi_m$ taken in $H = 100$ Oe for $RTiO_3$ with R = La, Pr, Nd, and Sm.

Table 2. Variation with R in $RTiO_3$ of magnetic parameters.

$RTiO_3$	T_{N1} (K)	T_{N2} (K)	T_C (K)	T_l (K)
La	140			
Pr	120	82		
Nd	110	80		
Sm	70	45		
Gd			32	179
Tb			49	170
Dy			60	150
Y			30	
Ho			56	135
Er			42	120
Tm			68	100
Yb			36	80
Lu			40	

the orthorhombic b axis that decreases in magnitude with increasing r_{3+}. The transition at $r_{3+} \approx 1.11$ Å is similar to that found by Marezio [17, 18] in the $RFeO_3$ family and has been interpreted [19] to be due to a distortion of the $MO_{6/2}$ octahedra that is superimposed on the cooperative site rotations as a result of R–O interactions that occur where an $r_{3+} > 1.11$ Å

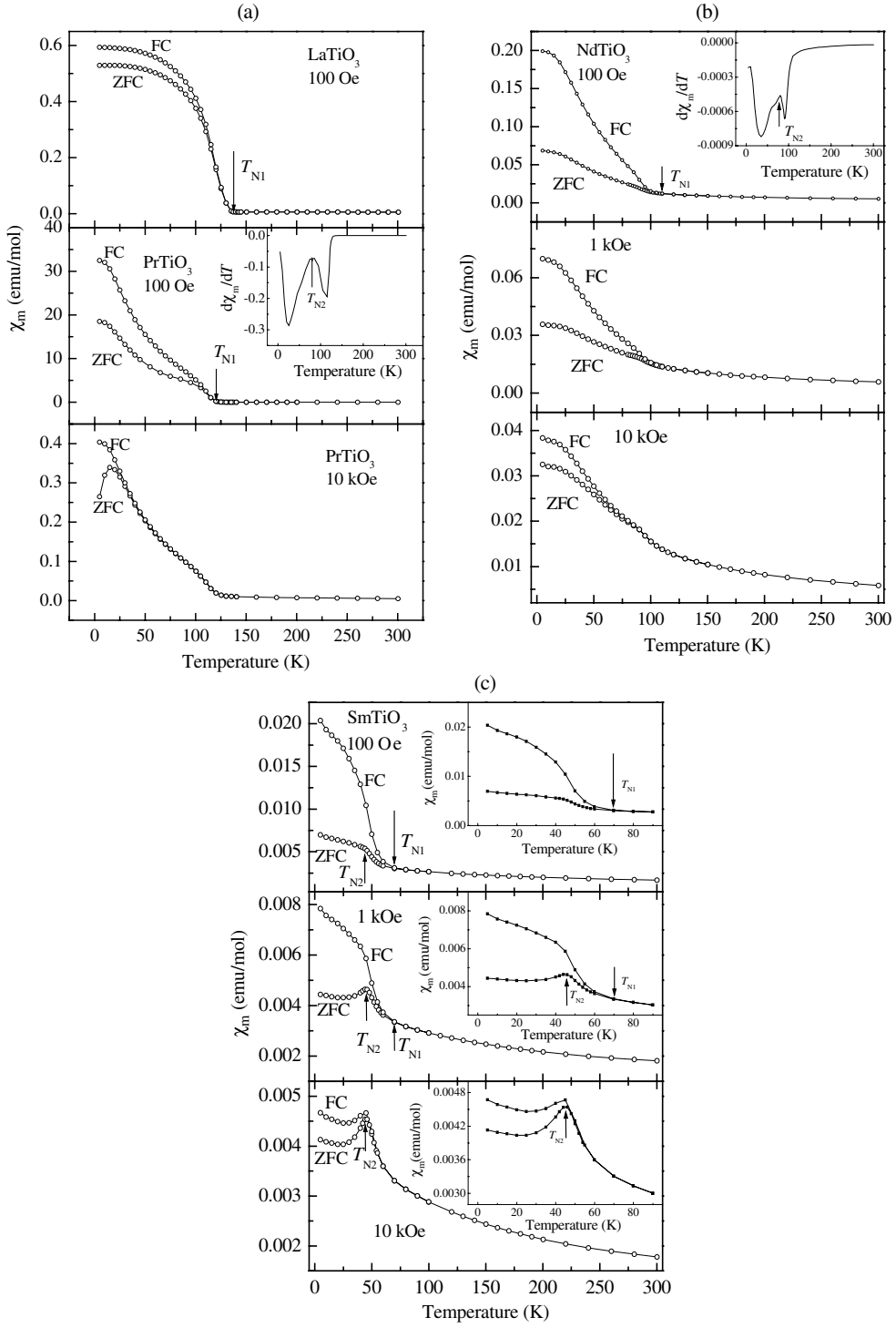

Figure 4. Molar magnetic susceptibility χ_m for (a) $LaTiO_3$ with $H = 100$ Oe, $PrTiO_3$ with $H = 100$ Oe, 10 kOe; (b) $NdTiO_3$ and (c) $SmTiO_3$ with $H = 100$ Oe, 1 kOe, and 10 kOe. Inset of (a) and (b): derivative of $\chi_m(T)$ for $PrTiO_3$ and $NdTiO_3$.

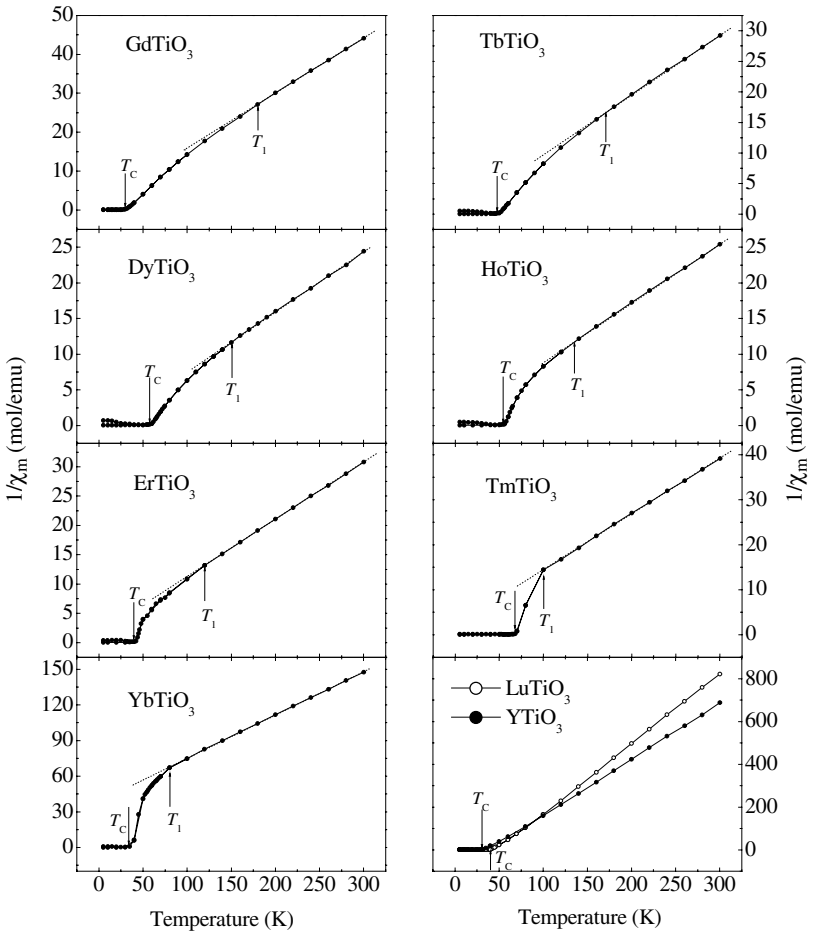

Figure 5. Inverse molar magnetic susceptibility $1/\chi_m$ for $RTiO_3$ (R = Gd–Lu, Y), taken in $H = 100$ Oe. The dashed lines are guides to the eye.

is found. This interpretation is consistent with the observation of Cwik *et al* [12] for the TiO_3 family. Accordingly, figure 1 shows that the unit-cell volume varies linearly with r_{3+} in accordance with Végard's law only in the region $r_{3+} < 1.13$ Å where $c/a > \sqrt{2}$ is found; for larger r_{3+}, a $c/a \leqslant \sqrt{2}$ signals that a $TiO_{6/2}$ octahedral-site deformation is superimposed on the rotation, and this deformation results in smaller volumes V for R = Nd, Pr, and La than is predicted by extrapolation of V versus r_{3+} from compounds with a smaller r_{3+}.

Since the site deformation has been found to be a general property of RMO_3 perovskites with $r_{3+} > 1.11$ Å where there is no orbital order, we may conclude that the site deformation is not driven by the orbital order; it is driven by the R^{3+}–O interactions caused by shortening of an R–O bond length in the RO rock-salt (001) planes by the octahedral-site rotation. The site deformations stabilize, in turn, an orbital ordering of the single d electron of a Ti atom into an a_1 orbital oriented along a site [111] axis, and the orbital order increases the magnitude of the site deformation. The strongly correlated electrons introduce a localized spin on the Ti^{3+} ions; antiferromagnetic a_1^1–O–a_1^1 interactions between half-filled a_1 orbitals below T_{N1} introduce an exchange striction that stabilizes further the orbital order, thereby enhancing the

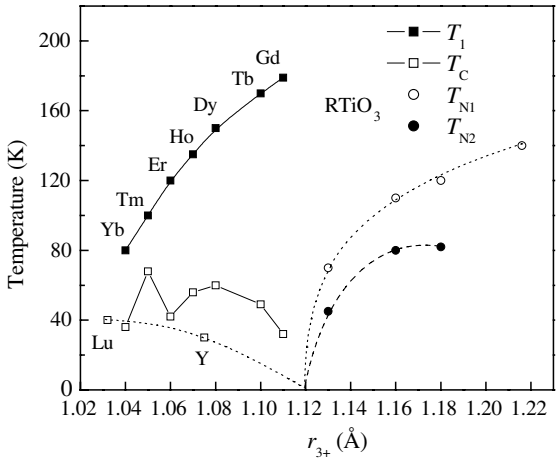

Figure 6. Transition temperatures T_1, T_C, T_{N1} and T_{N2} versus r_{3+} for $RTiO_3$. The dotted line is a guide to the eye of the Curie temperature for the $RTiO_3$ compounds without any moment on the R^{3+} ion, i.e. R = Lu and Y. The curve is extrapolated to zero at $Sm_{0.5}Gd_{0.5}TiO_3$ where there is a crossover from ferromagnetic to antiferromagnetic coupling within the TiO_3 array.

site deformation. However, as the initial site deformation is reduced by introduction of a smaller R^{3+} ion, stabilization of the a_1^1 configuration is more difficult, and T_{N1} decreases. Where the initial site deformation becomes negligible, the orbital order in the TiO_3 array is stabilized by a cooperative Jahn–Teller distortion that minimizes the elastic energy and maximizes the ferromagnetic interactions. Cooperative Jahn–Teller distortions are a characteristic of localized electrons, and their orbital-ordering temperature increases (not shown in figure 6) as the bandwidth of the Ti^{4+}/Ti^{3+} redox couple narrows.

The activation energies E_a of figure 2 for the smaller R^{3+} ions (R = Gd–Lu, Y) are typical for small-polaron conduction; those for the larger R^{3+} ions become increasingly smaller from Sm to La. As the transitions from strong to weak electron correlations in a single-valent parent compound is approached from the strong-correlation side, holes introduced into the occupied redox couple (lower Hubbard band) may not be confined to a single cation site, i.e. be self-trapped as a small dielectric polaron. For example, holes introduced into antiferromagnetic La_2CuO_4 either by Sr substitution for La or by the introduction of interstitial oxide ions form polarons occupying five to six Cu centres in a CuO_2 plane [20, 21]. These larger polarons have a smaller motional enthalpy because the oxygen displacements that define the polaron are smaller where the hole population per cation centre within the polaron is reduced [22]. Similarly, stoichiometric $LaTiO_3$ is close to the transition from strong to weak electron correlations, i.e. to the Mott–Hubbard transition, and we have interpreted thermoelectric-power data for p-type $LaTiO_3$ to reflect polaronic conduction with a polaron size approaching ten Ti centres in a 3D matrix [11]. The activation energy E_a for hole transport in $LaTiO_3$ is, therefore, small. In the $RTiO_3$ family, the bandwidth of the $RTiO_3$ couple decreases with decreasing r_{3+}, which should reduce the size of the polaron until, below a critical value of r_{3+}, it occupies only a single Ti site, i.e. is reduced to a small polaron. As the size of a polaron shrinks, the oxygen displacements that define it become larger, which increases the motional enthalpy ΔH_m. Once the size of the charge carriers is reduced to that of a small polaron, no further reduction in size can occur. Nevertheless, as the bandwidth of the redox energy decreases further, the electron localization becomes greater and E_a continues to increase, but less dramatically. From

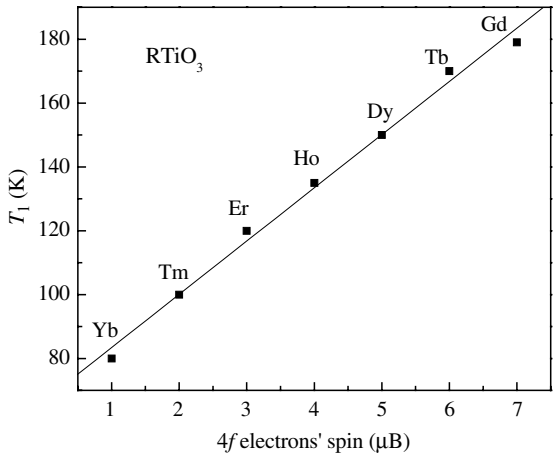

Figure 7. Variation of T_1 with the R^{3+}-ion spin.

these considerations, we interpret figure 2 to signal a reduction of the polaron size from that found in $LaTiO_3$ to that of a small polaron as r_{3+} decreases between $LaTiO_3$ and $GdTiO_3$. The narrowing of the redox bands is also manifest in an increase in the $(U - W)$ energy gap between the Ti^{4+}/Ti^{3+} and Ti^{3+}/Ti^{2+} couples (the lower and upper Hubbard bands) from 0.2 eV in $LaTiO_3$ to 1.2 eV in $YTiO_3$ [1, 2].

The $1/\chi_m(T)$ curve for $LaTiO_3$, figure 3, shows a Weiss constant with an anomalously large magnitude ($\theta = -853$ K) as well as too large a $\mu_{eff} = 2.43\ \mu_B$ for normal localized-electron behaviour; it has been accounted for by invoking orbital fluctuations [23], but it is also characteristic of itinerant-electron magnetism at the crossover to strongly correlated electrons. Below T_{N1}, the spins of the TiO_3 array order antiferromagnetically, but spin canting introduces a weak ferromagnetic component.

The large moments of the R^{3+} ions dominate the $1/\chi_m(T)$ curves for R = Pr, Nd, and Sm. Below T_{N1}, only the weak ferromagnetic component of the TiO_3 array introduces an R–O–Ti interaction, and the R–O–R interactions are stronger. Therefore, the rare-earth ions order antiferromagnetically below a $T_{N2} < T_{N1}$ [4, 5] where they introduce an additional canted-spin ferromagnetic component that couples to that of the TiO_3 array [24]. From the peak in the $d\chi_m(T)/dT$ curve, see the inset of figure 4, we determine a $T_{N2} = 82$, 80, and 45 K for R = Pr, Nd, and Sm, respectively. The larger divergence of the FC and ZFC $\chi_m(T)$ curves below T_{N2} reflects the large crystalline anisotropy of the R^{3+}-ion ferromagnetic component and its coupling to the ferromagnetic component of the TiO_3 array.

The R–O–Ti interactions are stronger than the R–O–R interactions where the TiO_3 array orders ferromagnetically, and an antiferromagnetic R–O–Ti interaction gives ferrimagnetic order below T_C [5]. Nevertheless, the $1/\chi_m(T)$ curves for the heavier rare earths, figure 5, show a deviation from Curie–Weiss behaviour only below a $T_1 > T_C$ that decreases smoothly with r_{3+}, figure 6. Figure 7 shows that T_1 decreases linearly with the spin on the R^{3+} ion. Therefore, we conclude that T_1 represents the onset of spin–spin coupling between the R^{3+} and Ti^{3+} ions in the paramagnetic phase. Figure 6 also shows that the coupling between the R^{3+} and Ti^{3+} spins tends to raise T_C above the value it would have were there no rare-earth spin, as is the case for R = Lu and Y. In addition, the larger T_C for $LuTiO_3$ than for $YTiO_3$ means that T_C increases as the bandwidth narrows, which is characteristic of itinerant-electron magnetism rather than of spin–spin interactions between localized-electron spins that are well

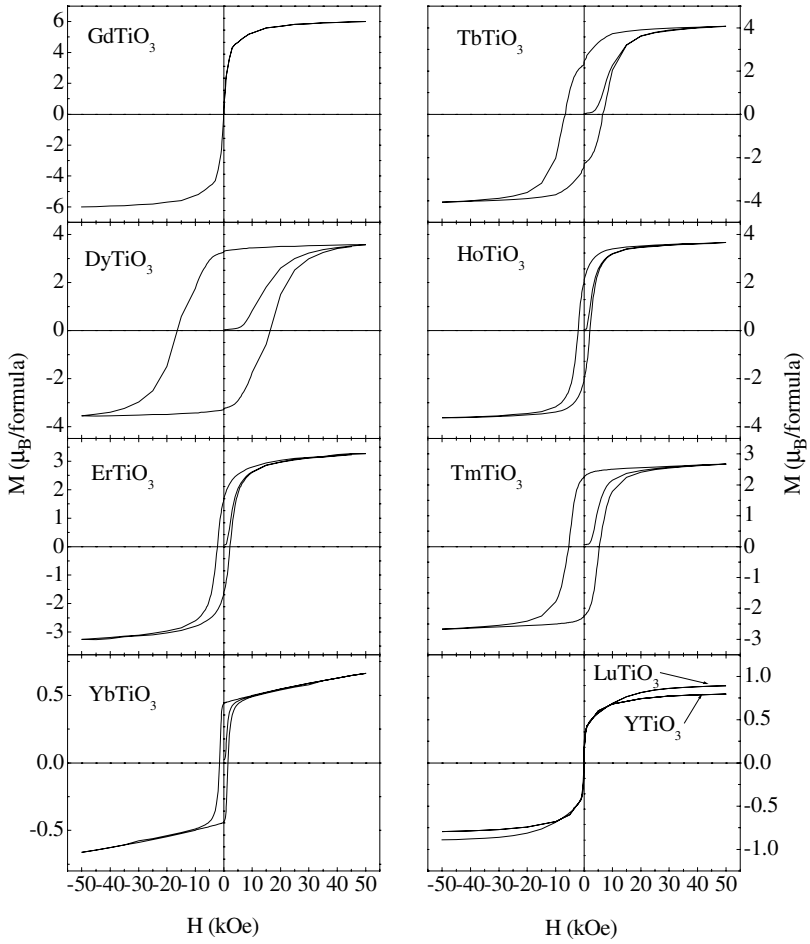

Figure 8. M–H hysteresis loops taken at 5 K for $RTiO_3$ (R = Gd–Lu, Y).

described by perturbation theory. Therefore, we turn finally to the magnitudes of the saturation magnetization to see whether $LuTiO_3$ has a ferromagnetic magnetization at $T = 5$ K that is closer to the spin-only value of 1 μ_B/Ti.

The M–H hysteresis loops of figure 8 show that at 5 K the saturation magnetization of $LuTiO_3$ reaches 0.9 μ_B/Ti whereas that of $YTiO_3$ is only 0.8 μ_B/Ti. On the other hand, an $M_s(5\text{ K}) = 6\ \mu_B$/Ti for $GdTiO_3$ corresponds to full spin-only ferrimagnetism; the Gd–O–Ti interaction both raises T_C and fully magnetizes the TiO_3 array. There is no evidence of an orbital contribution that lowers the magnetization of the TiO_3 array. Moreover, the M–H curves of the polycrystalline samples show no evidence of a large magnetocrystalline anisotropy. We are thus led to the conclusion that where there is no moment of the R^{3+} ion, the Ti–O–Ti spin–spin interaction of the strongly correlated electrons of the insulating, ferromagnetic TiO_3 array is not strong enough to remove completely the spin degeneracy of the Ti-3d electrons.

Also noteworthy in figure 8 are the small remanences and coercivities of $GdTiO_3$, $YTiO_3$, and $LuTiO_3$. As pointed out elsewhere [11], the G-type yz, zx orbital ordering of the ferromagnetic TiO_3 array is interrupted by antiphase boundaries across which the coupling is antiferromagnetic. Therefore, ferromagnetic blocks couple antiferromagnetically across these

boundaries in zero applied magnetic field, but a modest applied field exerts a high enough torque to align the blocks ferromagnetically provided there is no large magnetocrystalline anisotropy; the magnetocrystalline anisotropy associated with the R^{3+} ion and the R–O–Ti coupling inhibits rotation to give a large M–H hysteresis loop.

We found no evidence of 'cluster-glass' behaviour in any of our samples.

5. Conclusion

The orthorhombic ($Pbnm$) structure of the RMO_3 perovskites can be described by a cooperative rotation of the $MO_{6/2}$ octahedra about the b-axis if the R^{3+} ion has an ionic radius $r_{3+} < 1.11$ Å; but an R–O interaction for $r_{3+} > 1.11$ Å creates, in addition, a deformation of the $MO_{6/2}$ site to rhombohedral symmetry. Therefore, the stabilization of electronic charge along a site [111] axis in the $RTiO_3$ perovskites with R = La to Sm is driven by the site deformation, not by a cooperative Jahn–Teller orbital ordering. Occupancy of the a_1 orbitals is responsible for antiferromagnetic order on the TiO_3 array, and T_{N1} decreases as the site deformation responsible for preferential occupancy of an a_1 orbital decreases. On the other hand, the heavier R^{3+} ions and Y^{3+} have an $r_{3+} < 1.11$ Å, and in these $RTiO_3$ perovskites the Ti^{4+}/Ti^{3+} redox band is narrow enough to stabilize a cooperative Jahn–Teller orbital ordering; the G-type order of the occupied yz and zx orbitals introduces, as previously noted by others [10], ferromagnetic Ti–O–Ti interactions. Therefore, the change from antiferromagnetic to ferromagnetic order at an $r_{3+} \approx 1.11$ Å signals that the site deformations that determine the magnetic order are driven by cooperative Jahn–Teller orbital ordering for $r_{3+} < 1.11$ Å and by a structural site deformation for $r_{3+} > 1.11$ Å.

Holes introduced by a small cation (probably R^{3+}) deficiency are polaronic, but the size of the polarons progressively decrease with r_{3+} from roughly ten Ti atoms per hole in $LaTiO_3$ to small polarons as the bandwidth narrows to that of $GdTiO_3$.

The R–O–Ti spin–spin coupling is stronger than the R–O–R coupling in the ferrimagnetic $RTiO_3$ compounds with $r_{3+} < 1.11$ Å, but the R–O–R coupling is the stronger in the antiferromagnetic compounds having an $r_{3+} > 1.11$ Å. In the ferrimagnetic compounds, the strength of the R–O–Ti interactions is proportional to the magnitude of the R^{3+}-ion spin.

Although the electrons of the TiO_3 array are strongly correlated in all members of the $RTiO_3$ family, $LaTiO_3$ is close to the threshold for a transition to metallic behaviour and, in the absence of a spin on the R^{3+} ion, the saturation magnetization at 5 K of a ferromagnetic TiO_3 array increases with decreasing bandwidth of the Hubbard bands. Therefore, we conclude that the abnormal magnetic behaviour of $LaTiO_3$ reflects an itinerant-electron antiferromagnetism of the strongly correlated electrons. The Jahn–Teller cooperative orbital ordering and the apparent small-polaron behaviour found for compounds with $r_{3+} < 1.11$ Å would appear to signal localized-electron behaviour; the interatomic spin–spin interactions would then be described by a virtual charge transfer from a half-filled to an empty orbital in superexchange perturbation theory. However, in the absence of any evidence of a strong orbital magnetism or magnetocrystalline anisotropy of the TiO_3 array, the evidence for failure of the on-site electron–electron interactions to remove completely the spin degeneracy of the ferromagnetic Ti-3d electrons where there is no spin on the R^{3+} ions either implies an incomplete orbital ordering as a result of a phase separation into an orbitally ordered phase and an orbitally disordered phase that decreases in volume fraction as the lower Hubbard band narrows or it poses a challenge to the theorist to develop a more adequate description of the evolution of magnetic properties from the onset of a strong-correlation energy gap to localized-electron ferromagnetism.

Finally, we found no evidence for 'cluster-glass' behaviour in our samples where there was no variance of the R^{3+}-ion radius.

Acknowledgments

The NSF and the Robert A Welch Foundation of Houston, TX, are thanked for financial support.

References

[1] Goral J P, Greedan J E and MacLean D A 1982 *J. Solid State Chem.* **43** 244
[2] Okimoto Y, Katsufuji T, Okada Y, Arima T and Tokura Y 1995 *Phys. Rev.* B **51** 9581
[3] Onoda M and Kohno M 1998 *J. Phys.: Condens. Matter* **10** 1003
[4] Turner C W and Greedan J E 1980 *J. Solid State Chem.* **34** 207
[5] Turner C W, Collins M F and Greedan J E 1981 *J. Magn. Magn. Mater.* **23** 265
[6] Onoda M and Yasumoto M 1997 *J. Phys.: Condens. Matter* **9** 3861
[7] Onoda M and Yasumoto M 1997 *J. Phys.: Condens. Matter* **9** 5623
[8] Greedan J E 1985 *J. Less-Common Met.* **111** 335
[9] Amow G, Zhou J S and Goodenough J B 2000 *J. Solid State Chem.* **154** 619
[10] Itoh M, Tsuchiya M, Tanaka H and Motoya K 1999 *J. Phys. Soc. Japan* **68** 2783
[11] Zhou H D and Goodenough J B 2005 *Phys. Rev.* B **71** 184431
[12] Cwik M, Lorenz T, Baier J, Müller R, André G, Bourée F, Lichtenberg F, Freimuth A, Schmitz R, Müller-Hartmann E and Braden M 2003 *Phys. Rev.* B **68** 060401(R)
[13] Eremina R M, Eremin M V, Iglamov V V, Hemberger J, Krug von Nidda H A, Lichtenberg F and Loidl A 2004 *Phys. Rev.* B **70** 224428
[14] Yoshii K and Nakamura A 1998 *J. Solid State Chem.* **137** 181
Yoshii K, Nakamura A, Abe H and Morii Y 2000 *J. Solid State Chem.* **153** 145
Yoshii K, Nakamura A and Abe H 2000 *J. Alloys Compounds* **307** 25
[15] Goodenough J B, Zhou J S and Chan J 1993 *Phys. Rev.* B **47** 5275
[16] Zhou J S, Goodenough J B and Dabrowski B 2003 *Phys. Rev.* B **67** 020404(R)
[17] Marezio M, Remeika J P and Dernier P D 1970 *Acta Crystallogr.* B **26** 2008
[18] Marezio M and Dernier P D 1971 *Mater. Res. Bull.* **6** 23
[19] Zhou J S, Goodenough J B and Dabrowski B 2004 *Phys. Rev.* B **70** 081102(R)
[20] Zhou J S and Goodenough J B 1996 *Phys. Rev.* B **54** 12488
[21] Goodenough J B 2003 *J. Phys.: Condens. Matter* **15** R257
[22] Bersuker G I and Goodenough J B 1997 *Physica* C **274** 267
[23] Khaliullin G 2005 *Phys. Rev.* B **64** 212405
Kikoin K, Entin-Wohlmann O, Fleurov V and Aharony A 2003 *Phys. Rev.* B **67** 214418
[24] Greedan J E 1984 *J. Magn. Magn. Mater.* **44** 299